Chapter 2
Basic Concepts and Methodology

In this chapter, the main concepts relevant for the theoretical study of elementary photochemical processes are briefly reviewed. The notions of vibronic coupling and conical intersection are first introduced. The main basic tools from the molecular electronic structure theory and their use for the exploration of potential energy surfaces are then presented.

2.1 The Molecular Schrödinger Equation

2.1.1 The Molecular Hamiltonian Operator

The Hamiltonian operator $H(\boldsymbol{r}, \boldsymbol{R})$ of a molecule composed of N_{nu} nuclei and N_{el} electrons is the sum of a nuclear kinetic energy operator (KEO) $T_{nu}(\boldsymbol{R})$, an electronic KEO $T_{el}(\boldsymbol{r})$ and a potential energy operator $V(\boldsymbol{r}, \boldsymbol{R})$ that describes the Coulombic interaction between the different particles. Here, $\boldsymbol{r}$ and $\boldsymbol{R}$ denote vectors collecting all the electron and nuclear coordinates respectively. The KEOs read

$$T_{nu}(\boldsymbol{R}) = -\sum_{\alpha}^{N_{nu}} \frac{\hbar^2}{2M_\alpha} \boldsymbol{\nabla}_\alpha . \boldsymbol{\nabla}_\alpha \tag{2.1}$$

$$T_{el}(\boldsymbol{r}) = -\sum_{i}^{N_{el}} \frac{\hbar^2}{2m_e} \boldsymbol{\nabla}_i . \boldsymbol{\nabla}_i \tag{2.2}$$

where m_e is the mass of the electron, M_α is the mass of the αth nucleus and $\boldsymbol{\nabla}_i$ ($\boldsymbol{\nabla}_\alpha$) is a vector operator containing the derivative operators with respect to the coordinates of the ith electron (αth nucleus) as elements, i.e $\boldsymbol{\nabla}_i = \left(\frac{\partial}{\partial x_i}, \frac{\partial}{\partial y_i}, \frac{\partial}{\partial z_i}\right)$ in Cartesian coordinates. The potential operator is the sum of an electron–electron repulsion operator, a nucleus–nucleus repulsion operator and an electron–nucleus

M. Sala, *Quantum Dynamics and Laser Control for Photochemistry*,
Springer Theses, DOI 10.1007/978-3-319-28979-3_2

attraction operator

$$V(\boldsymbol{r}, \boldsymbol{R}) = \sum_{i}^{N_{el}} \sum_{j>i}^{N_{el}} \frac{e^2}{4\pi\varepsilon_0 |\boldsymbol{r}_j - \boldsymbol{r}_i|} + \sum_{\alpha}^{N_{nu}} \sum_{\beta>\alpha}^{N_{nu}} \frac{Z_\alpha Z_\beta e^2}{4\pi\varepsilon_0 |\boldsymbol{R}_\alpha - \boldsymbol{R}_\beta|} - \sum_{\alpha}^{N_{nu}} \sum_{i}^{N_{el}} \frac{Z_\alpha e^2}{4\pi\varepsilon_0 |\boldsymbol{R}_\alpha - \boldsymbol{r}_i|}, \tag{2.3}$$

where Z_α is the charge of the αth nucleus, e is the electron charge, $\boldsymbol{r}_i$ and $\boldsymbol{R}_\alpha$ are the position vectors of the ith electron and αth nucleus, respectively.

The quantum mechanical description of a molecule requires the solution of the time-dependent Schrödinger equation (TDSE) associated with the Hamiltonian operator $H(\boldsymbol{r}, \boldsymbol{R}) = T_{nu}(\boldsymbol{R}) + T_{el}(\boldsymbol{r}) + V(\boldsymbol{r}, \boldsymbol{R})$ described above

$$H(\boldsymbol{r}, \boldsymbol{R})\Psi(\boldsymbol{r}, \boldsymbol{R}, t) = i\hbar \frac{\partial}{\partial t} \Psi(\boldsymbol{r}, \boldsymbol{R}, t). \tag{2.4}$$

Because the motions of the various particles are correlated through the potential terms of Eq. (2.3), the direct integration of the molecular Schrödinger equation is an extremely difficult task that is only possible, in practice, for the simplest atomic and molecular systems.

2.1.2 The Born–Oppenheimer Approximation

The above problem can be simplified by separating the fast electronic motion from the slow nuclear motion. One first defines an electronic Hamiltonian, also called clamped nucleus Hamiltonian $H_{el}(\boldsymbol{r}; \boldsymbol{R}) = T_{el}(\boldsymbol{r}) + V(\boldsymbol{r}; \boldsymbol{R})$. This electronic Hamiltonian acts in the electronic space and depends parametrically on the nuclear coordinates $\boldsymbol{R}$, as indicated by the semicolon in the coordinate dependence of the operators. The eigenfunctions and eigenvalues of the associated time-independent Schrödinger equation (TISE)

$$H_{el}(\boldsymbol{r}; \boldsymbol{R})\phi_n(\boldsymbol{r}; \boldsymbol{R}) = V_n(\boldsymbol{R})\phi_n(\boldsymbol{r}; \boldsymbol{R}) \tag{2.5}$$

are the electronic adiabatic energies and eigenfunctions. The set of eigenfunctions $\{\phi_n(\boldsymbol{r}; \boldsymbol{R})\}$ satisfies the usual orthonormality relation

$$\langle \phi_m | \phi_n \rangle = \int \phi_m^*(\boldsymbol{r}; \boldsymbol{R})\phi_n(\boldsymbol{r}; \boldsymbol{R}) d\boldsymbol{r} = \delta_{mn}. \tag{2.6}$$

The molecular wavefunction $\Psi(\boldsymbol{r}, \boldsymbol{R}, t)$ of Eq. (2.4) can be expanded in the basis of the electronic eigenfunctions

$$\Psi(\boldsymbol{r}, \boldsymbol{R}, t) = \sum_n \chi_n(\boldsymbol{R}, t)\phi_n(\boldsymbol{r}; \boldsymbol{R}). \tag{2.7}$$

The exact molecular TDSE then reads

$$T_{nu}\sum_n \chi_n(\boldsymbol{R},t)\phi_n(\boldsymbol{r};\boldsymbol{R}) + H_{el}\sum_n \chi_n(\boldsymbol{R},t)\phi_n(\boldsymbol{r};\boldsymbol{R}) = i\hbar\frac{\partial}{\partial t}\sum_n \chi_n(\boldsymbol{R},t)\phi_n(\boldsymbol{r};\boldsymbol{R}). \tag{2.8}$$

Let us, for simplicity, rewrite the nuclear kinetic energy operator in terms of mass-weighted rectilinear coordinates (defined as the rectilinear coordinates multiplied by the square root of the mass of the nucleus) $T_{nu} = -\frac{\hbar^2}{2}\boldsymbol{\nabla}_{\boldsymbol{R}}.\boldsymbol{\nabla}_{\boldsymbol{R}}$. The first term of the last equation can now be developed

$$\begin{aligned} T_{nu}\sum_n \chi_n(\boldsymbol{R},t)\phi_n(\boldsymbol{r};\boldsymbol{R}) = \sum_n \big[&\chi_n(\boldsymbol{R},t)T_{nu}\phi_n(\boldsymbol{r};\boldsymbol{R}) + \phi_n(\boldsymbol{r};\boldsymbol{R})T_{nu}\chi_n(\boldsymbol{R},t) \\ &- \hbar^2\boldsymbol{\nabla}_{\boldsymbol{R}}\phi_n(\boldsymbol{r};\boldsymbol{R}).\boldsymbol{\nabla}_{\boldsymbol{R}}\chi_n(\boldsymbol{R},t)\big]. \end{aligned} \tag{2.9}$$

Inserting Eq. (2.9) in Eq. (2.8), multiplying from the left by $\phi_m^*(\boldsymbol{r};\boldsymbol{R})$ and integrating over the electronic coordinates, one obtains

$$\left[T_{nu} + V_m(\boldsymbol{R})\right]\chi_m(\boldsymbol{R},t) + \sum_n \Lambda_{mn}\chi_n(\boldsymbol{R},t) = i\hbar\frac{\partial}{\partial t}\chi_m(\boldsymbol{R},t). \tag{2.10}$$

This last equation shows that the nuclear motion of the molecule obeys an infinite set of coupled differential equations. The so-called *non-adiabatic couplings* Λ_{mn} describe the dynamical interaction between the electronic and nuclear motions [1–3]. They are given by

$$\Lambda_{mn} = \boldsymbol{F}_{mn}.\boldsymbol{\nabla}_{\boldsymbol{R}} + G_{mn} \tag{2.11}$$

where $\boldsymbol{F}_{mn} = -\hbar^2\langle\phi_m|\boldsymbol{\nabla}_{\boldsymbol{R}}\phi_n\rangle$ is a non-adiabatic *derivative coupling vector* element and $G_{mn} = \langle\phi_m|T_{nu}|\phi_n\rangle = -\frac{\hbar^2}{2}\langle\phi_m|\nabla_R^2\phi_n\rangle$ is an element of the non-adiabatic *scalar couplings*. The derivative coupling vector matrix $\boldsymbol{F}$ is antihermitian, i.e $\boldsymbol{F}^\dagger = -\boldsymbol{F}$. If the adiabatic electronic wavefunctions $\phi_n(\boldsymbol{r};\boldsymbol{R})$ are chosen to be real, then the diagonal elements of $\boldsymbol{F}$ vanish.

The Born–Oppenheimer approximation [4, 5] consists in neglecting the non-adiabatic couplings. This approximation relies on the very different masses of the electron and nuclei. Indeed, the proton, which is the lightest atomic nucleus, is roughly 1836 times heavier than the electron. Therefore the electron velocity is much higher than that of the nuclei and the fast electrons adjust instantaneously to the slow motion of the nuclei. Within this approximation, no transition between different adiabatic electronic states can be induced by the nuclear motion and in this case, the total molecular wavefunction can be written as

$$\Psi(\boldsymbol{r},\boldsymbol{R},t) = \chi(\boldsymbol{R},t)\phi(\boldsymbol{r};\boldsymbol{R}), \tag{2.12}$$

which leads to

$$\left[T_{nu} + V(\boldsymbol{R}) + \Lambda\right]\chi(\boldsymbol{R},t) = i\hbar\frac{\partial}{\partial t}\chi(\boldsymbol{R},t). \tag{2.13}$$

Equation (2.13) constitutes the Born–Oppenheimer approximation. When the electronic adiabatic wavefunctions are chosen real, the non-adiabatic term simply reads $\Lambda = G = \langle\phi|T_{nu}|\phi\rangle$. Usually, Λ is very small and Eq. (2.13) is only used if very high accuracy is sought. Neglecting Λ leads to the so-called adiabatic approximation

$$[T_{nu} + V(\boldsymbol{R})]\,\chi(\boldsymbol{R}, t) = i\hbar\frac{\partial}{\partial t}\chi(\boldsymbol{R}, t). \tag{2.14}$$

Below, we show that the validity of the adiabatic approximation is directly related to the energy separation between the different electronic states. To this purpose, a useful expression for the derivative coupling vectors $\boldsymbol{F}_{mn}$ can be derived. It follows directly from the electronic TISE

$$\langle\phi_m|H_{el}|\phi_n\rangle = V_n(\boldsymbol{R})\delta_{mn}. \tag{2.15}$$

Applying the nuclear gradient on both sides, one obtains

$$\boldsymbol{\nabla}_{\boldsymbol{R}}\langle\phi_m|H_{el}|\phi_n\rangle = \boldsymbol{\nabla}_{\boldsymbol{R}}V_n(\boldsymbol{R})\delta_{mn}. \tag{2.16}$$

Let us develop the left hand side of this last equation

$$\begin{aligned}\boldsymbol{\nabla}_{\boldsymbol{R}}\langle\phi_m|H_{el}|\phi_n\rangle &= \langle\boldsymbol{\nabla}_{\boldsymbol{R}}\phi_m|H_{el}|\phi_n\rangle + \langle\phi_m|(\boldsymbol{\nabla}_{\boldsymbol{R}}H_{el})|\phi_n\rangle + \langle\phi_m|H_{el}|\boldsymbol{\nabla}_{\boldsymbol{R}}\phi_n\rangle \\ &= (V_m(\boldsymbol{R}) - V_n(\boldsymbol{R}))\langle\phi_m|\boldsymbol{\nabla}_{\boldsymbol{R}}\phi_n\rangle + \langle\phi_m|(\boldsymbol{\nabla}_{\boldsymbol{R}}H_{el})|\phi_n\rangle. \end{aligned}\tag{2.17}$$

From the last two equations, one finally obtains

$$\boldsymbol{F}_{mn} = \frac{\langle\phi_m|(\boldsymbol{\nabla}_{\boldsymbol{R}}H_{el})|\phi_n\rangle - \boldsymbol{\nabla}_{\boldsymbol{R}}V_n(\boldsymbol{R})\delta_{mn}}{V_n(\boldsymbol{R}) - V_m(\boldsymbol{R})}. \tag{2.18}$$

For $m = n$, we have seen above that by choosing the $\phi_n(\boldsymbol{r}; \boldsymbol{R})$ real, the $\boldsymbol{F}_{nn}$ term vanishes. For $m \neq n$,

$$\boldsymbol{F}_{mn} = \frac{\langle\phi_m|(\boldsymbol{\nabla}_{\boldsymbol{R}}H_{el})|\phi_n\rangle}{V_n(\boldsymbol{R}) - V_m(\boldsymbol{R})}. \tag{2.19}$$

This last equation shows that the magnitude of the non-adiabatic coupling vector depends on the energy separation between the different electronic states. They become large when different electronic states become close in energy. In particular, the non-adiabatic coupling vector diverges in the situation where two or more electronic states are degenerate. This particular situation is called a *conical intersection*, and leads to a breakdown of the adiabatic approximation near the degeneracy.

2.2 Vibronic Coupling

2.2.1 The Group Born–Oppenheimer Approximation

As seen in the previous section, the separability of the electronic and nuclear motions rests both on the large difference between the masses of electrons and nuclei and on a sufficient energetic separation between the electronic states. When electronic states become close in energy, the corresponding non-adiabatic coupling matrix elements become large and the Born–Oppenheimer approximation breaks down. However, in such situations, one is usually interested in a few electronic states and the couplings between them. Therefore one can consider a block of electronic states inside of which the non-adiabatic couplings are taken into account, and neglect the couplings between the states of interest and the other states. Considering a block of N_{st} states of interest, the set of equations of motion for the nuclei of Eq. (2.10) reduces to

$$[T_{nu} + V_m(\boldsymbol{R})]\,\chi_m(\boldsymbol{R}, t) + \sum_n^{N_{st}} \Lambda_{mn}\chi_n(\boldsymbol{R}, t) = i\hbar\frac{\partial}{\partial t}\chi_m(\boldsymbol{R}, t), \tag{2.20}$$

where the indices n and m span the group of states of interest. Obviously, as for the original Born–Oppenheimer approximation, this partitioning of the space of the electronic states is only valid if the energy separation between the electronic states of interest and the higher electronic states is sufficient. This approximation is known as the group Born–Oppenheimer approximation [3].

2.2.2 The Diabatic Representation

Although the group Born–Oppenheimer approximation greatly simplifies the description of molecular systems with strong vibronic interactions between low-lying electronic states, Eq. (2.20) is still difficult to handle when the electronic states are nearly degenerate because of the divergence of the derivative couplings $\boldsymbol{F}_{mn}$, and of the topography of the adiabatic potential energy surfaces (PESs), which are difficult to represent by simple mathematical expressions. Therefore, in general, a more convenient representation of the electronic states, called *diabatic representation*, is used in quantum dynamical investigations. The diabatic representation is constructed such as to provide smooth potential energy and coupling surfaces. The diabatic basis is obtained through a unitary transformation

$$\boldsymbol{\phi^d}(\boldsymbol{r}; \boldsymbol{R}) = \boldsymbol{S}(\boldsymbol{R})\boldsymbol{\phi}(\boldsymbol{r}; \boldsymbol{R}), \tag{2.21}$$

where $\boldsymbol{\phi} = (\phi_1, \phi_2, \ldots, \phi_{N_{st}})^T$ and similarly $\boldsymbol{\phi^d} = (\phi_1^d, \phi_2^d, \ldots, \phi_{N_{st}}^d)^T$, such that the derivative couplings in the new representation are zero

$$\boldsymbol{F}^{\boldsymbol{d}}_{\boldsymbol{mn}} = \langle \phi^d_m | \boldsymbol{\nabla}_{\boldsymbol{R}} \phi^d_n \rangle = 0. \tag{2.22}$$

The diabatic derivative coupling matrix can be expressed in the adiabatic representation as

$$\boldsymbol{F}^{\boldsymbol{d}} = \boldsymbol{S}^{\dagger} \boldsymbol{F} \boldsymbol{S} + \boldsymbol{S}^{\dagger} \boldsymbol{\nabla} \boldsymbol{S} \tag{2.23}$$

with $\boldsymbol{F} = [F_{mn}]$. It follows immediately that the unitary transformation that fulfills $\boldsymbol{F}^{\boldsymbol{d}} = 0$ satisfies the following equation:

$$\boldsymbol{F} \boldsymbol{S} + \boldsymbol{\nabla} \boldsymbol{S} = 0. \tag{2.24}$$

Unfortunately, in the general case of a polyatomic molecule, the last equation only has a solution if the complete set of adiabatic electronic states is considered. Therefore, in practice, a strict diabatic basis does not exist and one usually searches a quasidiabatic representation that makes the derivative couplings small enough to be safely neglected. Several methods have been proposed to obtain a quasidiabatic representation from ab initio computed data in the adiabatic representation. These methods, which are reviewed in the Chap. 4 of Ref. [6], can be classified into three classes, depending on the type of data used to construct the quasidiabatic representation. The first class contains derivative-based methods, which use ab initio computed derivative couplings to integrate directly Eq. (2.24). These methods require the computation of the derivative couplings over extended portions of the geometry space and are therefore computationally expansive. The second class contains property-based methods, which attempt to reduce the configurational change of the electronic wavefunctions upon geometry changes to determine the transformation matrix $\boldsymbol{S}$. Since smoother electronic states yield smoother properties, this can also be achieved by enforcing the smoothness of electronic properties, such as, for instance, the dipole moment. The last class contains energy-based methods, which use only ab initio computed electronic energies.

Assuming that a suitable quasidiabatic representation has been derived, the TDSE in the diabatic representation can be written in matrix form as

$$[T_{nu} \boldsymbol{I} + \boldsymbol{W}(\boldsymbol{R})] \boldsymbol{\chi}^{\boldsymbol{d}}(\boldsymbol{R}, t) = i\hbar \frac{\partial}{\partial t} \boldsymbol{\chi}^{\boldsymbol{d}}(\boldsymbol{R}, t), \tag{2.25}$$

where

$$\boldsymbol{\chi}^{\boldsymbol{d}}(\boldsymbol{R}, t) = \boldsymbol{S}(\boldsymbol{R}) \boldsymbol{\chi}(\boldsymbol{R}, t), \tag{2.26}$$

is the vector of the diabatic nuclear wavefunction components and

$$\boldsymbol{W}(\boldsymbol{R}) = \boldsymbol{S}^{\dagger}(\boldsymbol{R}) \boldsymbol{V}(\boldsymbol{R}) \boldsymbol{S}(\boldsymbol{R}) \tag{2.27}$$

is the matrix of the diabatic potentials with

$$W_{mn} = \langle \phi^d_m | H_{el} | \phi^d_n \rangle. \tag{2.28}$$

We note that the diabatic electronic states are no longer eigenstates of the electronic Schrödinger equation, which means that the diabatic potential matrix is not diagonal. This transformed nuclear TDSE has a much more appealing form than the original nuclear TDSE in the adiabatic representation of Eq. (2.20) because the couplings between the different diabatic electronic states now appear in the diabatic potential matrix $\boldsymbol{W}(\boldsymbol{R})$ that contains only local, i.e scalar, operators. In addition, in practice, the diabatic potential and coupling surfaces have a much simpler topography than their adiabatic counterparts.

2.2.3 Conical Intersections

The diabatic representation can now be used to characterize the topography of the PESs at the vicinity of conical intersections. We first expand the diabatic potential energy matrix elements as Taylor expansions around a reference geometry $\boldsymbol{R_0}$

$$\boldsymbol{W}(\boldsymbol{R}) = \boldsymbol{W^{(0)}} + \boldsymbol{W^{(1)}} + \boldsymbol{W^{(2)}} + \cdots . \tag{2.29}$$

It is assumed that the diabatic representation has been constructed such that, at this point, the adiabatic and diabatic representations are identical. This is always possible since Eq. (2.24) defines the transformation $\boldsymbol{S}(\boldsymbol{R})$ up to a constant unitary transformation. In other words, if the matrix $\boldsymbol{S}(\boldsymbol{R})$ satisfies Eq. (2.24), the matrix $\boldsymbol{T}\boldsymbol{S}(\boldsymbol{R})$, where $\boldsymbol{T}$ does not depends on $\boldsymbol{R}$, also does. Therefore, by choosing $\boldsymbol{T} = \boldsymbol{S}^{\dagger}(\boldsymbol{R}_0)$, the adiabatic and diabatic representations are identical at $\boldsymbol{R}_0$. This point can be the ground state equilibrium geometry, a point of electronic degeneracy, or any other point of interest. The zeroth order diabatic potential matrix is simply the diagonal matrix of the adiabatic energies

$$W_{ij}^{(0)} = \langle \phi_i | H_{el} | \phi_j \rangle \big|_{\boldsymbol{R}_0} = V_i(\boldsymbol{R}_0)\delta_{ij}. \tag{2.30}$$

The first order potential matrix can be expressed in the adiabatic basis at $\boldsymbol{R}_0$ as

$$W_{ij}^{(1)}(\boldsymbol{R}) = \left[\langle \phi_i | \nabla_{\boldsymbol{R}} H_{el} | \phi_j \rangle \big|_{\boldsymbol{R}_0} \right]^T (\boldsymbol{R} - \boldsymbol{R}_0). \tag{2.31}$$

For diagonal elements, this leads to

$$\begin{aligned} W_{ii}^{(1)}(\boldsymbol{R}) &= \left[\langle \phi_i | \nabla_{\boldsymbol{R}} H_{el} | \phi_i \rangle |_{\boldsymbol{R}_0} \right]^T (\boldsymbol{R} - \boldsymbol{R}_0) \\ &= \left[\nabla_{\boldsymbol{R}} \langle \phi_i | H_{el} | \phi_i \rangle |_{\boldsymbol{R}_0} \right]^T (\boldsymbol{R} - \boldsymbol{R}_0) \\ &= \nabla_{\boldsymbol{R}} V_i(\boldsymbol{R})|_{\boldsymbol{R}_0}^T (\boldsymbol{R} - \boldsymbol{R}_0), \end{aligned} \tag{2.32}$$

where we have used the fact that the diagonal elements of the $\boldsymbol{F}$ matrix are zero for real electronic wavefunctions. One can see from this last equation that the gradients

of the adiabatic PESs at the reference geometry $\boldsymbol{R}_0$ appear in $W_{ii}^{(1)}(\boldsymbol{R})$. In addition, the non-diagonal elements $W_{ij}^{(1)}(\boldsymbol{R})$ are related to the derivative couplings given in Eq. (2.19).

The adiabatic potential energy matrix $\boldsymbol{V}(\boldsymbol{R})$ is obtained by diagonalizing the diabatic potential energy matrix $\boldsymbol{W}(\boldsymbol{R})$, through the unitary transformation $\boldsymbol{S}(\boldsymbol{R})$ introduced in Eq. (2.21)

$$\boldsymbol{V}(\boldsymbol{R}) = \boldsymbol{S}(\boldsymbol{R})\boldsymbol{W}(\boldsymbol{R})\boldsymbol{S}^{\dagger}(\boldsymbol{R}). \tag{2.33}$$

Considering a two-state system, the adiabatic PESs read

$$V_{1,2}(\boldsymbol{R}) = \frac{1}{2}(W_{11}(\boldsymbol{R}) + W_{22}(\boldsymbol{R})) \mp \frac{1}{2}\sqrt{(W_{22}(\boldsymbol{R}) - W_{11}(\boldsymbol{R}))^2 + 4W_{12}(\boldsymbol{R})^2}. \tag{2.34}$$

We now truncate the expansion of Eq. (2.29) to first order and consider $\boldsymbol{R_0}$ to be a point of degeneracy. Introducing the following notations: $\boldsymbol{Q} = \boldsymbol{R} - \boldsymbol{R_0}$, $W_{ii}^{(1)}(\boldsymbol{Q}) = \boldsymbol{\kappa}^{(i)}.\boldsymbol{Q}$ and $W_{12}^{(1)}(\boldsymbol{Q}) = \boldsymbol{\lambda}.\boldsymbol{Q}$, the adiabatic PESs read

$$V_{1,2}(\boldsymbol{Q}) = \frac{1}{2}(\boldsymbol{\kappa}^{(1)} + \boldsymbol{\kappa}^{(2)}).\boldsymbol{Q} \mp \frac{1}{2}\sqrt{(\boldsymbol{\delta}.\boldsymbol{Q})^2 + 4(\boldsymbol{\lambda}.\boldsymbol{Q})^2}, \tag{2.35}$$

where $\boldsymbol{\delta} = \boldsymbol{\kappa^{(2)} - \kappa^{(1)}}$. From this last equation, the conditions for the existence of a conical intersection between the two adiabatic PESs are:

$$\boldsymbol{\delta}.\boldsymbol{Q} = 0 \quad \text{and} \quad \boldsymbol{\lambda}.\boldsymbol{Q} = 0. \tag{2.36}$$

Therefore, at first order, the degeneracy is lifted along two directions defined by the unitary vectors

$$\boldsymbol{e}_g = \frac{\boldsymbol{g}}{||\boldsymbol{g}||} = \frac{\nabla_Q(\boldsymbol{\delta}.\boldsymbol{Q})}{||\nabla_Q(\boldsymbol{\delta}.\boldsymbol{Q})||} = \frac{\boldsymbol{\delta}}{||\boldsymbol{\delta}||}, \tag{2.37}$$

and

$$\boldsymbol{e}_h = \frac{\boldsymbol{h}}{||\boldsymbol{h}||} = \frac{\nabla_Q(\boldsymbol{\lambda}.\boldsymbol{Q})}{||\nabla_Q(\boldsymbol{\lambda}.\boldsymbol{Q})||} = \frac{\boldsymbol{\lambda}}{||\boldsymbol{\lambda}||}. \tag{2.38}$$

In these last equations, $\boldsymbol{g} = \boldsymbol{\delta}$ is the *gradient difference* vector and $\boldsymbol{h} = \boldsymbol{\lambda}$ is the linear *derivative coupling* vector. The space spanned by these two vectors is called the $g-h$ space or branching space whereas the space orthogonal to the branching space is the intersection space, also called conical intersection seam. Thus, a conical intersection is a subspace of the nuclear configuration space of dimension 3N-8, where N denotes the number of atoms of the system (the space of the nuclear configurations is of dimension 3N-6).

From Eq. (2.35), the adiabatic PESs form a double cone at the intersection, as illustrated in Fig. 2.1. Any infinitesimal displacement along a direction orthogonal to the branching space preserves the degeneracy. However we stress that, because

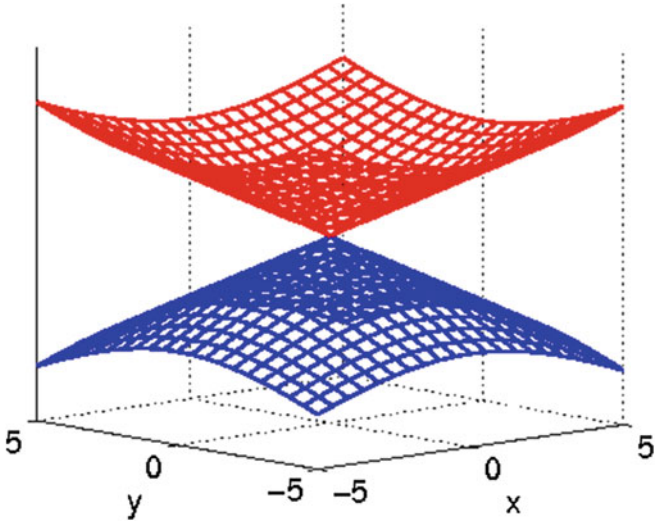

Fig. 2.1 Adiabatic PESs around a conical intersection obtained within the first-order description. The PESs are obtained from Eq. (2.34) with $W_{11} = -x$, $W_{22} = x$ and $W_{12} = y$. V_1 and V_2 are displayed in *blue* and *red*, respectively

of the first order nature of the above analysis, a finite displacement along such a direction will in general lift the degeneracy. This is a consequence of the curvature of the conical intersection seam, encapsulated in the second order terms $\boldsymbol{W}^{(2)}$ in Eq. (2.29) [7–9].

2.3 Basics of Electronic Structure Theory

In the previous section, we have seen that in a vast majority of cases, the quantum mechanical description of a molecular system can be greatly simplified if the nuclear and electronic motions are separated. In this case, the electronic problem can be treated for fixed nuclei by solving the clamped nucleus or electronic TISE of Eq. (2.5). Finding accurate and efficient numerical procedures to solve the electronic TISE has been a major goal of theoretical chemistry since the beginning of the second part of the previous century [10, 11].

2.3.1 Spin Orbitals and Slater Determinants

In quantum mechanics, to completely describe an electron, the spin needs to be considered in addition to its motion in space. Electrons have a spin $s = \frac{1}{2}$,

therefore the electron spin state space is spanned by the orthonormal basis $\left\{|s=\frac{1}{2}, m_s=\frac{1}{2}\rangle, |s=\frac{1}{2}, m_s=-\frac{1}{2}\rangle\right\}$ conventionally noted $\{|\alpha\rangle, |\beta\rangle\}$. It is often convenient, for ease of notation, to introduce an unspecified spin variable, that we note σ, and to represent the eigenstates $|\alpha\rangle$ and $|\beta\rangle$ by eigenfunctions $\langle\sigma|\alpha\rangle = \alpha(\sigma)$ and $\langle\sigma|\beta\rangle = \beta(\sigma)$. It follows that an electron will be specified by four variables, the three spatial variables, gathered in the vector $\boldsymbol{r}$ and the spin variable. These will be conveniently gathered in a vector $\boldsymbol{\xi} \equiv (\boldsymbol{r}, \sigma)$. In general, the wavefunction of a single electron $\psi(\boldsymbol{\xi})$ is called a spin orbital. It is expressed as the product of a function of the spatial coordinates $\boldsymbol{r}$ named spatial orbital and one of the two spin functions

$$\psi(\boldsymbol{\xi}) = \varphi(\boldsymbol{r}) \times \begin{cases} \alpha(\sigma) \\ \text{or} \\ \beta(\sigma) \end{cases} . \tag{2.39}$$

From a set of K spatial orbitals, a set of $2K$ spin orbitals can be generated. In addition, if the spatial orbitals are orthonormal, so are the spin orbitals. In the rest of this chapter, the spin orbitals will be called molecular orbitals (MOs).

The wavefunction of a N-electron system must be antisymmetric with respect to the exchange of two electrons

$$\Psi\left(\boldsymbol{\xi_1}, \ldots, \boldsymbol{\xi_i}, \ldots, \boldsymbol{\xi_j}, \ldots, \boldsymbol{\xi_N}\right) = -\Psi\left(\boldsymbol{\xi_1}, \ldots, \boldsymbol{\xi_j}, \ldots, \boldsymbol{\xi_i}, \ldots, \boldsymbol{\xi_N}\right). \tag{2.40}$$

A wavefunction satisfying this requirement can be conveniently written in the form of a Slater determinant [12]

$$\Phi(\boldsymbol{\xi_1}, \boldsymbol{\xi_2}, \ldots, \boldsymbol{\xi_N}) = \frac{1}{\sqrt{N!}} \begin{vmatrix} \psi_1(\boldsymbol{\xi_1}) & \psi_2(\boldsymbol{\xi_1}) & \cdots & \psi_N(\boldsymbol{\xi_1}) \\ \psi_1(\boldsymbol{\xi_2}) & \psi_2(\boldsymbol{\xi_2}) & \cdots & \psi_N(\boldsymbol{\xi_2}) \\ \vdots & \vdots & \ddots & \vdots \\ \psi_1(\boldsymbol{\xi_N}) & \psi_2(\boldsymbol{\xi_N}) & \cdots & \psi_N(\boldsymbol{\xi_N}) \end{vmatrix} . \tag{2.41}$$

The factor $\frac{1}{\sqrt{N!}}$ ensures the normalization of the Slater determinant. As seen in Eq. (2.41), the coordinates of a single electron appear in a given row whereas a single MO appears in a given column. According to the general properties of determinants, the exchange of the coordinates of two electrons correspond to the permutation of two rows of the determinant, which changes its sign. Therefore the Slater determinant satisfies the antisymmetry principle, illustrated by Eq. (2.40). In addition, if two MOs are identical, two of the columns of the determinant are identical, which makes it zero. This correspond to the physical situation of two electron being in the same quantum state. Thus we see that the antisymmetry principle implies that two fermions can not be in the same quantum state. This principle is known as the Pauli exclusion principle.

2.3.2 The Hartree–Fock Approximation

The Hartree–Fock approximation [13, 14] plays a central role in the molecular electronic structure theory. In most cases, it provides a qualitatively correct description of the electronic structure of many electron atoms and molecules in their ground electronic state. In addition, it constitutes a basis upon which more accurate methods can be developed. A detailed derivation and discussion of the method can be found in textbooks such as [10, 11]. The Hartree–Fock approximation assumes the simplest possible form for the electronic wavefunction, i.e a single Slater determinant given by Eq. (2.41). Starting from the electronic TISE Eq. (2.5), the Hartree–Fock energy E^{HF} is simply

$$E^{HF} = \langle \Phi | H_{el} | \Phi \rangle. \tag{2.42}$$

The Hartree–Fock approximation relies on the variational principle, which states that any approximate wavefunction has an energy above or equal to the exact ground state energy. This principle has an important consequence: for a given system, the wavefunction of the form of Eq. (2.41) that minimizes the energy in Eq. (2.42) is the best possible wavefunction within the single determinant approximation.

Let us write the electronic Hamiltonian in atomic units

$$H_{el}(\boldsymbol{r};\boldsymbol{R}) = -\frac{1}{2}\sum_{i}^{N_{el}} \nabla_{\boldsymbol{i}}.\nabla_{\boldsymbol{i}} + \sum_{i}^{N_{el}}\sum_{j>i}^{N_{el}} \frac{1}{|\boldsymbol{r}_j - \boldsymbol{r}_i|} - \sum_{\alpha}^{N_{nu}}\sum_{i}^{N_{el}} \frac{Z_\alpha}{|\boldsymbol{R}_\alpha - \boldsymbol{r}_i|} + \sum_{\alpha}^{N_{nu}}\sum_{\beta>\alpha}^{N_{nu}} \frac{Z_\alpha Z_\beta}{|\boldsymbol{R}_\alpha - \boldsymbol{R}_\beta|}. \tag{2.43}$$

This Hamiltonian can be written as the sum of three operators

$$H_{el}(\boldsymbol{r};\boldsymbol{R}) = O^1(\boldsymbol{r};\boldsymbol{R}) + O^2(\boldsymbol{r}) + V^{NR}(\boldsymbol{R}), \tag{2.44}$$

where

$$O^1(\boldsymbol{r};\boldsymbol{R}) = \sum_{i}^{N_{el}} h_i \tag{2.45}$$

with

$$h_i = -\frac{1}{2}\nabla_{\boldsymbol{i}}.\nabla_{\boldsymbol{i}} - \sum_{\alpha}^{N_{nu}} \frac{Z_\alpha}{|\boldsymbol{R}_\alpha - \boldsymbol{r}_i|} \tag{2.46}$$

is a mono-electronic operator,

$$O^2(\boldsymbol{r}) = \sum_{i}^{N_{el}}\sum_{j>i}^{N_{el}} g_{ij} \tag{2.47}$$

with

$$g_{ij} = \frac{1}{|\boldsymbol{r}_j - \boldsymbol{r}_i|} \tag{2.48}$$

is a bi-electronic operator, and

$$V^{NR}(\boldsymbol{R}) = \sum_{\alpha}^{N_{nu}} \sum_{\beta>\alpha}^{N_{nu}} \frac{Z_\alpha Z_\beta}{|\boldsymbol{R}_\alpha - \boldsymbol{R}_\beta|} \tag{2.49}$$

is the nuclear repulsion potential energy operator. This last operator does not depend on the electronic coordinates and therefore contributes to the molecular energy as a constant.

With these definitions, the Slater–Condon rules [12, 15] can be used to obtain an expression for the energy of Eq. (2.42) as a function of the MOs. The contribution of the mono-electronic operator reads

$$\langle \Phi | O^1 | \Phi \rangle = \sum_{i}^{N_{el}} \langle \psi_i(\boldsymbol{\xi_1}) | h_1 | \psi_i(\boldsymbol{\xi_1}) \rangle. \tag{2.50}$$

The contribution of the bi-electronic operators reads

$$\begin{aligned} \langle \Phi | O^2 | \Phi \rangle &= \sum_{i}^{N_{el}} \sum_{j>i}^{N_{el}} \left(\langle \psi_i(\boldsymbol{\xi_1}) \psi_j(\boldsymbol{\xi_2}) | g_{12} | \psi_i(\boldsymbol{\xi_1}) \psi_j(\boldsymbol{\xi_2}) \rangle - \langle \psi_i(\boldsymbol{\xi_1}) \psi_j(\boldsymbol{\xi_2}) | g_{12} | \psi_j(\boldsymbol{\xi_1}) \psi_i(\boldsymbol{\xi_2}) \rangle \right) \\ &= \frac{1}{2} \sum_{i}^{N_{el}} \sum_{j}^{N_{el}} \left(J_{ij} - K_{ij} \right). \end{aligned} \tag{2.51}$$

In this last equation, J_{ij} and K_{ij} denote the Coulomb and exchange integrals, respectively. The Coulomb integral represents the repulsion between the two electronic densities $|\psi_i(\boldsymbol{\xi_1})|^2$ and $|\psi_j(\boldsymbol{\xi_2})|^2$. The exchange integral has no classical analogue and is a consequence of the Pauli principle. Using Eqs. (2.50) and (2.51), the Hartree–Fock energy reads

$$E^{HF} = \sum_{i}^{N_{el}} \langle \psi_i(\boldsymbol{\xi_1}) | h_1 | \psi_i(\boldsymbol{\xi_1}) \rangle + \frac{1}{2} \sum_{i}^{N_{el}} \sum_{j}^{N_{el}} (J_{ij} - K_{ij}) + V_{NR}(\boldsymbol{R}). \tag{2.52}$$

The above equation can be recast in a form where the Coulomb and exchange integrals are replaced by the expectation values of Coulomb and exchange operators J_i and K_i, defined such that

$$J_i | \psi_j(\boldsymbol{\xi_2}) \rangle = \langle \psi_i(\boldsymbol{\xi_1}) | g_{12} | \psi_i(\boldsymbol{\xi_1}) \rangle | \psi_j(\boldsymbol{\xi_2}) \rangle \tag{2.53}$$

and

$$K_i | \psi_j(\boldsymbol{\xi_2}) \rangle = \langle \psi_i(\boldsymbol{\xi_1}) | g_{12} | \psi_j(\boldsymbol{\xi_1}) \rangle | \psi_i(\boldsymbol{\xi_2}) \rangle. \tag{2.54}$$

The energy now reads

$$E^{HF} = \sum_{i}^{N_{el}} \langle \psi_i(\boldsymbol{\xi_1}) | h_1 | \psi_i(\boldsymbol{\xi_1}) \rangle + \frac{1}{2} \sum_{i}^{N_{el}} \sum_{j}^{N_{el}} \langle \psi_j(\boldsymbol{\xi_1}) | J_i - K_i | \psi_j(\boldsymbol{\xi_1}) \rangle + V_{NR}(\boldsymbol{R})$$
$$\equiv \sum_{i}^{N_{el}} \langle \psi_i | h_1 | \psi_i \rangle + \frac{1}{2} \sum_{i}^{N_{el}} \sum_{j}^{N_{el}} \langle \psi_j | J_i - K_i | \psi_j \rangle + V_{NR}(\boldsymbol{R}). \tag{2.55}$$

In this last equation, the dependence of the orbitals on the electronic coordinates is dropped since it formally depends on the coordinates of a single electron.

The objective is now to find the set of MOs that minimizes the energy of Eq. (2.55), with the additional constraint that the set of MOs remains orthonormal. This type of constrained optimization problem can be conveniently solved by the method of Lagrange multipliers. This method consists in minimizing the Lagrange function $\mathcal{L}$

$$\mathcal{L} = E - \sum_{i}^{N_{el}} \sum_{j}^{N_{el}} \varepsilon_{ij} (\langle \psi_i | \psi_j \rangle - \delta_{ij}) \tag{2.56}$$

with respect to the MOs

$$\delta \mathcal{L} = \delta E - \sum_{i}^{N_{el}} \sum_{j}^{N_{el}} \varepsilon_{ij} (\langle \delta\psi_i | \psi_j \rangle - \langle \psi_i | \delta\psi_j \rangle) = 0, \tag{2.57}$$

where the ε_{ij} are the Lagrange multipliers.

By developing this last equation, one finds the Hartree–Fock equations

$$F_i | \psi_i \rangle = \sum_{j} \varepsilon_{ij} | \psi_j \rangle \tag{2.58}$$

where F_i is an effective one-electron operator called the Fock operator

$$F_i = h_i + \sum_{j}^{N_{el}} \left(J_j - K_j \right). \tag{2.59}$$

The Fock operator is the sum of two terms: an operator h_i containing the kinetic energy operator and the electron–nuclei attraction potential operator, and an operator describing the repulsion of the electron with all the other electrons.

The matrix of the Lagrange multipliers $\boldsymbol{\varepsilon}$ is hermitian, therefore there exists a unitary transformation $\boldsymbol{U}$ that diagonalizes $\boldsymbol{\varepsilon}$. Applying this unitary transformation to the set of MOs $\{|\psi_i\rangle\}$

$$|\psi_i'\rangle = \sum_{j} U_{ij} | \psi_j \rangle \tag{2.60}$$

yields a new set of MOs $\{|\psi_i'\rangle\}$ verifying

$$F_i'|\psi_i'\rangle = \varepsilon_i'|\psi_i'\rangle \tag{2.61}$$

where $\boldsymbol{\varepsilon'} = \boldsymbol{U}^\dagger \boldsymbol{\varepsilon} \boldsymbol{U}$. In addition, it can be shown that $F_i' = F_i$ and that the electronic wavefunction constructed with the new MOs is equal to the original electronic wavefunction to a phase factor. This transformed set of equations is known as the *canonical Hartree–Fock equations* and the corresponding orbitals the *canonical orbitals*. The prime symbols will be dropped from now on. In this representation, the Lagrangian multiplier are interpreted as orbital energies

$$\langle\psi_i|F_i|\psi_i\rangle = \varepsilon_i\langle\psi_i|\psi_i\rangle = \varepsilon_i. \tag{2.62}$$

Equation (2.61) forms a set of pseudo-eigenvalue equations as the Fock operator depends on the MOs via the Coulomb and exchange operators, and must be solved by an iterative procedure. The unknown MOs $\{|\psi_i\rangle\}$ are expanded in a set of non-orthogonal, atom-centered basis functions $|\psi_i\rangle = \sum_\mu c_{\mu i}|\chi_\mu\rangle$. Inserting this expansion in the canonical Hartree–Fock equations Eq. (2.61) yields

$$F_i \sum_\mu c_{\mu i}|\chi_\mu\rangle = \varepsilon_i \sum_\mu c_{\mu i}|\chi_\mu\rangle. \tag{2.63}$$

Multiplying on the left by χ_ν^* and integrating, one obtains

$$\sum_\mu c_{\mu i}\langle\chi_\nu|F_i|\chi_\mu\rangle = \varepsilon_i \sum_\mu c_{\mu i}\langle\chi_\nu|\chi_\mu\rangle. \tag{2.64}$$

This last set of equations can be written in a compact matrix form

$$\boldsymbol{FC} = \boldsymbol{SC\varepsilon} \tag{2.65}$$

where $\boldsymbol{F}$ is the Fock matrix of elements $F_{\nu\mu} = \langle\chi_\nu|F_i|\chi_\mu\rangle$, $\boldsymbol{S}$ is the overlap matrix of elements $S_{\nu\mu} = \langle\chi_\nu|\chi_\mu\rangle$ and $\boldsymbol{C}$ is the vector of the coefficients of the expansion of the MOs on the basis set $c_{\mu i} = \langle\chi_\mu|\psi_i\rangle$. These equations are known as the *Roothaan–Hall equations* [16, 17]. The problem of the calculation of the MOs is now turned into the determination of the coefficients $c_{\mu i}$.

The presence of the overlap matrix $\boldsymbol{S}$ in the Roothaan–Hall equations Eq. (2.65) reflects the fact that the basis functions used to expand the orbitals are non-orthogonal. By multiplying from the left by $\boldsymbol{S}^{-\frac{1}{2}}$ and inserting the unit matrix $\boldsymbol{I} = \boldsymbol{S}^{-\frac{1}{2}}\boldsymbol{S}^{\frac{1}{2}}$, Eq. (2.65) can be recast as

$$\tilde{\boldsymbol{F}}\tilde{\boldsymbol{C}} = \tilde{\boldsymbol{C}}\boldsymbol{\varepsilon}, \tag{2.66}$$

where $\tilde{\boldsymbol{F}} = \boldsymbol{S}^{-\frac{1}{2}}\boldsymbol{F}\boldsymbol{S}^{-\frac{1}{2}}$ and $\tilde{\boldsymbol{C}} = \boldsymbol{S}^{\frac{1}{2}}\boldsymbol{C}$. Equation (2.66) is a standard set of eigenvalue equations, the diagonalization of the matrix $\tilde{\boldsymbol{F}}$ yields a set of eigenvectors $\tilde{\boldsymbol{C}}$ which can be back-transformed to obtain the vectors $\boldsymbol{C}$ solutions of Eq. (2.65).

As mentioned above, since the construction of the Fock matrix $\boldsymbol{F}$ involves the calculation of integrals over the Coulomb and exchange operators which depend on the MOs that we want to calculate, the Roothaan–Hall equations must be solved iteratively. The procedure starts with the definition of an initial guess for the MOs. This can be done conveniently by using simple empirical methods such as the Hückel method [18]. Using this initial guess, the Fock matrix can be constructed and diagonalized to yield a new set of MOs which is in turn used to construct a new Fock matrix. This procedure, called the Self-Consistent Field (SCF) method, is iterated until convergence of the MOs.

For a N-electron closed-shell molecule, using a basis containing $M \geq N$ functions, the solution of the Roothaan–Hall equations generates M spatial orbitals and $2M$ spin orbitals. In the case of molecule with an even number of electrons and a singlet ground state (a closed-shell molecule), the restriction that each spatial orbital should have two electrons (one with spin α and one with spin β) is usually made. This method is called *restricted Hartree–Fock* method. In this case, among the M spatial orbitals obtained from the calculation, the $N/2$ orbitals of lowest energy are occupied and the remaining $M - N/2$ MOs are unoccupied, or virtual orbitals. The Hartree–Fock energy and the N-electron wavefunction are obtained using the $N/2$ occupied orbitals. This description defines the notion of an electronic configuration associated with a Slater determinant, which correspond to a particular repartition of the electrons in the different MOs.

In most cases, the Hartree–Fock method provides a qualitatively correct description of the electronic structure of a molecular system. Usually, the Hartree–Fock method gives 99 % of the total energy of the molecule described by the non-relativistic Schrödinger equation and the clamped nucleus Hamiltonian. The difference between the best Hartree–Fock energy, i.e the Hartree–Fock energy in the limit of an infinite basis, and the "exact" energy is called the electronic correlation energy.

2.3.3 Electronic Correlation

Taking into account the electronic correlation is mandatory if a quantitative description of the electronic structure and energy of the system of interest is required. In addition, in some cases, the inclusion of the electronic correlation effects are necessary to obtain even a qualitatively correct description of the electronic structure of the system. By definition, the mean-field approximation resulting from the approximation of the multi-electron wavefunction by a single Slater determinant is unable to account for the electronic correlation. A correlated electronic wavefunction must then be written as a linear combination of several Slater determinants

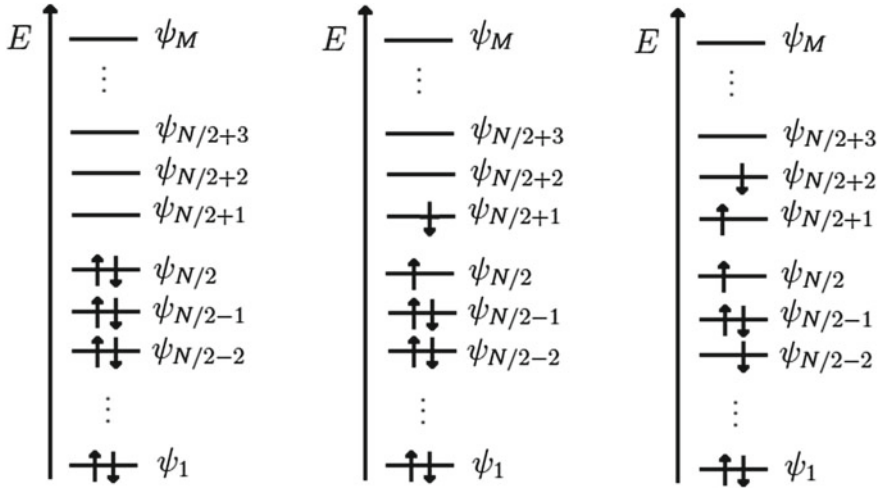

Fig. 2.2 Scheme illustrating different electronic configuration for a molecular system of N electrons described in a basis of M orbitals. The *left scheme* shows the ground state configuration, the *middle scheme* shows a singly excited configuration and the *right scheme* a doubly excited configuration

$$\Psi(\boldsymbol{\xi_1}, \boldsymbol{\xi_2}, \ldots, \boldsymbol{\xi_N}) = \sum_i c_i \Phi_i(\boldsymbol{\xi_1}, \boldsymbol{\xi_2}, \ldots, \boldsymbol{\xi_N}). \tag{2.67}$$

From a set of orbitals such as the one obtained from a Hartree–Fock calculation, many Slater determinants corresponding to excited configurations can be constructed. These are obtained by replacing one or several occupied orbitals by virtual orbitals, as illustrated in Fig. 2.2.

Usually, two different types of electronic correlation are distinguished, the *static electronic correlation* and the *dynamic electronic correlation*. Although this distinction is by no means strict, it is useful because the two types of electronic correlation have different physical origins and different methods can be used to recover one or the other type of correlation.

A strong static correlation is encountered in situations where several electronic states are degenerate, or at least close in energy. Such situations occur when electrons can be distributed in several ways in orbitals close in energy. This is the case, for instance, in bond breaking processes, or in the case of systems containing transition metal atoms with incomplete electronic shells. The electronic wavefunction will therefore include important contributions from a few configurations, and the Hartree–Fock method has to be replaced by a method capable of treating several configurations on an equal footage. This is the case of the Multi-Configuration Self-consistent field (MCSCF) method, in which the trial wavefunction is expressed as a linear combination of Slater determinants as in Eq. (2.67), and both the MOs and expansion coefficients c_i are optimized variationally.

The dynamic electronic correlation results from the Coulombic repulsion between two electrons lying close to each other. It requires the inclusion of a large number of configurations obtained by exciting electrons to high-energy virtual orbitals. However, in this case the electronic structure is still dominated by a single configuration and the other Slater determinants included in the wavefunction have small coefficients. Therefore the dynamic correlation energy can be recovered by methods starting from the Hartree–Fock wavefunction. Among the methods that are able to take into account the dynamic correlation energy, one can cite the configuration interaction methods (CI), methods based on the perturbation theory or the coupled cluster methods (CC). These methods are usually qualified as *single-reference* methods because they start from the Hartree–Fock Slater determinant.

Unfortunately, in many situation of interest, both static and dynamic electronic correlation need to be taken into account. This is particularly true for the study of processes involving excited electronic states as in UV spectroscopy or in photochemistry. In this case, methods capable of taking into account the dynamic electronic correlation on top of a multi-determinantal wavefunction of the MCSCF type are needed. These methods are usually called *multi-reference* methods. The two standard methods that are able to account for both the static and dynamic electronic correlation are the multi-reference configuration interaction (MRCI) and several variants of second-order multi-reference perturbation theory (MRPT).

2.3.3.1 The Configuration Interaction Methods

In the configuration interaction method, the wavefunction is expanded in a basis of Slater determinants. The Hartree–Fock determinant, noted Φ^{HF}, is taken as a reference zeroth-order wavefunction. Slater determinants corresponding to excited configurations are generated by swapping occupied MOs ψ_a with virtual (unoccupied) MOs ψ_r and can be classified with respect to the number of excited electrons. Singly excited Slater determinants are noted Φ_a^r, doubly excited Slater determinants Φ_{ab}^{rs}, triply excited Slater determinants Φ_{abc}^{rst}, and so on. The configuration interaction wavefunction then reads

$$\begin{aligned}\Psi &= c_{HF}\Phi^{HF} + \sum_{a,r} c_{ar}\Phi_a^r + \sum_{a<b,r<s} c_{ab,rs}\Phi_{ab}^{rs} + \cdots \\ &= \sum_I c_I \Phi_I \end{aligned} \tag{2.68}$$

where I is a composite index accounting for all kinds of excitations. The final configuration interaction wavefunction is obtained by variationally optimizing the expansion coefficients c_I, with the normalization constraint $\langle\Psi|\Psi\rangle$=1. Again, this is done by using the Lagrange multiplier technique. The Lagrangian function

$$\begin{aligned}\mathcal{L} &= \langle\Psi|H|\Psi\rangle - E(\langle\Psi|\Psi\rangle - 1) \\ &= \sum_I \sum_J c_I^* c_J \langle\Phi_I|H|\Phi_J\rangle - E\left(\sum_I c_I^* c_I - 1\right)\end{aligned} \tag{2.69}$$

is minimized with respect to the expansion coefficients

$$\frac{\partial \mathcal{L}}{\partial c_I} = 2\sum_J c_J \langle\Phi_I|H|\Phi_J\rangle - 2Ec_I = 0. \tag{2.70}$$

This last set of equations can be written in matrix form

$$\boldsymbol{Hc} = \boldsymbol{Ec}. \tag{2.71}$$

Solving this set of secular equations is equivalent to diagonalizing the configuration interaction matrix $\boldsymbol{H}$. Therefore the lowest eigenvalue of $\boldsymbol{H}$ is the ground state energy, the second lowest, the energy of the first excited state, and so on.

When all the Slater determinants that can be constructed from a set of Hartree–Fock MOs are taken into account, the method is called full configuration interaction. It provides the best possible solutions of the non-relativistic, clamped nuclei TISE within the basis set used for the calculation. The exact solutions are thus obtained from a full configuration interaction calculation at the complete basis limit. However, the number of configurations that can be built from a set of MOs grows extremely fast with the size of the system (i.e the size of the molecule and/or of the basis set).

For most systems, it is therefore necessary to reduce the number of configurations. This is usually done by truncating the expansion of Eq. (2.68) to a given level of excitation. When only singly excited configurations are included, the method is called configuration interaction with single excitations (CIS). Because, in virtue of the Brillouin's theorem [10], matrix elements between the Hartree–Fock determinant and a singly excited determinant are zero, the CIS method does not improve the description of the ground electronic state. It allows one to calculate excited states that are dominated by single excitations with an accuracy similar to that of the Hartree–Fock method for the ground state.

Including the singly and doubly excited configurations yields the configuration interaction with single and double excitations method (CISD). In contrast to the CIS method, the CISD method improves the description of the ground state because doubly excited configurations are directly mixed with the Hartree–Fock configuration

$$\langle\Phi^{HF}|H_{el}|\Phi_{ab}^{rs}\rangle = \langle\psi_a\psi_b|g_{12}|\psi_r\psi_s\rangle - \langle\psi_a\psi_b|g_{12}|\psi_s\psi_r\rangle. \tag{2.72}$$

In addition, in the CISD method, the singly excited configurations are now indirectly mixed to the ground state, through their mixing with the doubly excited configurations. Configuration interaction methods including higher level excitations (CISDT, CISDTQ, ...) are less commonly used.

2.3.3.2 The Multi-configuration Self-consistent Field Method

The Multi-Configuration Self-Consistent Field method combines the ideas of orbital optimization through a SCF technique as in the Hartree–Fock method, and a multi-configuration expansion of the electronic wavefunction as in the configuration interaction method. In other words, the electronic wavefunction is still expressed as a linear combination of Slater determinants $\Psi = \sum_i c_i \Phi_i$, but now both the coefficients c_i and the orbitals are optimized variationally [19–22]. This procedure being computationally more expansive than the configuration interaction method, only a limited number of configurations can be included in the MCSCF wavefunction. Therefore, the MCSCF method is usually not used to calculate a large fraction of the dynamic electronic correlation energy. On the other hand, it is well suited when the static correlation effects are important. In these cases, several configurations are quasi-degenerate and need to be included in the electronic wavefunction on an equal footing to obtain a qualitatively correct zeroth order description of the electronic structure of the system.

An important issue in MCSCF calculations is the selection of the configurations to be included in the wavefunction expansion. The most popular approach is the complete active space self-consistent field (CASSCF) method, also called full optimized reaction space (FORS). This approach starts from a zeroth order set of MOs, usually obtained via the Hartree–Fock method. The set of MOs is split into three subsets, as illustrated in Fig. 2.3. A first one containing occupied inactive orbitals, for which the occupation numbers are fixed to 2. A second one containing active orbitals, including both occupied and virtual orbitals of the reference Hartree–Fock configuration, in which all possible electron excitations are allowed. And a third one containing virtual inactive orbitals, for which the occupation numbers are fixed to 0.

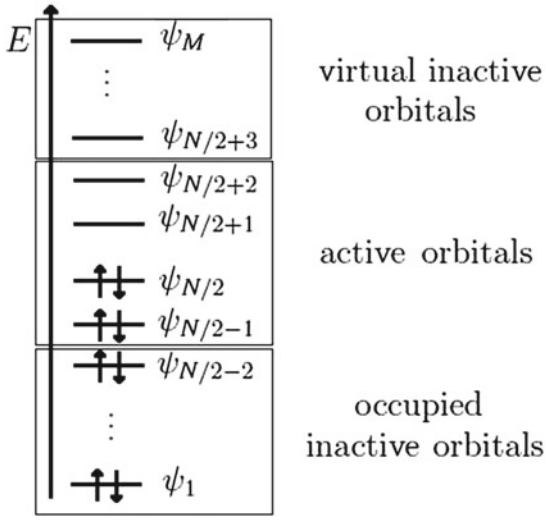

Fig. 2.3 Scheme illustrating the notion of active space in the CASSCF method. In the present case, an active space of four electrons in four orbitals, noted CAS(4, 4) is depicted

More precisely, a set of active orbitals and a number of active electrons are defined. All the configurations that can be built by excitations of the active electrons among the active orbitals are included into the wavefunction. Other, more flexible approaches for the selection of the configurations included in the MSCSF wavefunction exist, such as the *Restricted Active Space Self-Consistent Field* [23, 24] (RASSCF) and the *Occupation Restricted Multiple Active Space* (ORMAS) [25] methods.

A CASSCF wavefunction is, in general, much harder to converge than a simple SCF wavefunction. Several optimization procedures have been developed for the CASSCF wavefunction. The most popular one uses a Newton–Raphson-based method to minimize the energy. The energy is expanded to second order in the variational parameters (the orbital and configurational coefficients) around a particular set of coefficients

$$E(\boldsymbol{c}) = E(\boldsymbol{c_0}) + \boldsymbol{g}^T(\boldsymbol{c} - \boldsymbol{c_0}) + \frac{1}{2}(\boldsymbol{c} - \boldsymbol{c_0})^T \boldsymbol{H}(\boldsymbol{c} - \boldsymbol{c_0}). \tag{2.73}$$

In this equation, $\boldsymbol{c} \equiv \begin{pmatrix} \boldsymbol{c}^{(o)} \\ \boldsymbol{c}^{(c)} \end{pmatrix}$ is a vector gathering the orbital and configurational coefficients, $\boldsymbol{c_0}$ is the vector of the current coefficients, $\boldsymbol{g} = \nabla_{\boldsymbol{c}} E(\boldsymbol{c})|_{\boldsymbol{c}=\boldsymbol{c_0}}$ is the gradient of the energy with respect to the coefficients at $\boldsymbol{c_0}$ and $\boldsymbol{H} = \nabla_{\boldsymbol{c}} \nabla_{\boldsymbol{c}}{}^T E(\boldsymbol{c})\big|_{\boldsymbol{c}=\boldsymbol{c_0}}$ the Hessian matrix. Requiring the gradient of the energy to vanish yields

$$\boldsymbol{c} = \boldsymbol{c_0} - \boldsymbol{H}^{-1}\boldsymbol{g}. \tag{2.74}$$

Since the energy is not a quadratic function of the coefficients, several Newton steps are needed to locate a minimum. In addition, the calculation and inversion of the full Hessian matrix can be extremely time consuming for large active spaces and/or basis sets. Often, the elements of the Hessian coupling orbital and configurational coefficients (cross derivatives) are neglected and the optimization of the two sets of coefficients are decoupled.

During a CASSCF optimization near an electronic state degeneracy, problems of convergence often occur. The algorithm can swap from one state to the other. This problem is known as the root flipping problem. A way around this problem is to optimize the two states simultaneously. Specifically, a weighted average of the energies of the two states is minimized, and a same set of orbitals is optimized for the two states. This procedure is called state-averaged CASSCF (SA-CASSCF).

2.3.3.3 Methods Based on Perturbation Theory

As explained above, the dynamic electronic correlation can be taken into account by the (truncated) configuration interaction method in the case of a single reference system. Similarly, the multi-reference configuration interaction (MRCI) method can be used for multi-reference systems. In this method, a CASSCF wavefunction is used as the zeroth order description of the system. A configuration interaction matrix

containing all the configurations corresponding to single and double excitations (this is the MRCISD approach) from the configurations present in the CASSCF wavefunction is constructed and diagonalized. However this approach is computationally highly expansive and can only be used for small molecules.

Another approach is to include the effect of excited configurations through perturbation theory. This method avoids the diagonalization of a large matrix and can be accurate if the dynamic electronic correlation effects are not too large.

The Møller–Plesset perturbation theory [26] corresponds to the application of the stationary perturbation theory to the calculation of the correlation energy using the Hartree–Fock Slater determinant Φ^{HF} as the zeroth order wavefunction. These methods are denoted MPn where n is the order of the perturbative corrections included. In the Møller–Plesset method, the unperturbed Hamiltonian operator is chosen as a sum of Fock operators

$$H_0 = \sum_i^{N_{el}} F_i = \sum_i^{N_{el}} \left(h_i + \sum_j^{N_{el}} J_j - K_j \right). \tag{2.75}$$

The Hartree–Fock determinant and all Slater determinants built with Hartree–Fock orbitals are eigenfunctions of H_0. The perturbation operator W is then defined as the difference between H_0 and the exact electronic Hamiltonian H_{el} of Eq. (2.43)

$$W = H_{el} - H_0 = \sum_i^{N_{el}} \left(\sum_{j>i}^{N_{el}} g_{ij} - \sum_j^{N_{el}} J_j - K_j \right). \tag{2.76}$$

With these definitions, the zeroth order energy is a sum of MO energies

$$E_0^{(0)} = \langle \Phi^{HF} | H_0 | \Phi^{HF} \rangle = \sum_i^{N_{el}} \langle \Phi^{HF} | F_i | \Phi^{HF} \rangle = \sum_i^{N_{el}} \varepsilon_i. \tag{2.77}$$

The first order energy

$$E^{\mathrm{MP1}} = E_0^{(0)} + E_0^{(1)} = \langle \Phi^{HF} | H_0 | \Phi^{HF} \rangle + \langle \Phi^{HF} | W | \Phi^{HF} \rangle = \langle \Phi^{HF} | H_{el} | \Phi^{HF} \rangle = E^{HF} \tag{2.78}$$

is simply the Hartree–Fock energy. The general expression of the second order perturbative correction to the energy is:

$$E_0^{(2)} = \sum_{j \neq 0} \frac{|\langle \Phi^{HF} | W | \Phi_j \rangle|^2}{E_0^{(0)} - E_j^{(0)}} \tag{2.79}$$

where Φ_j denotes the excited Slater determinants. Singly excited determinants $\Phi_j \equiv \Phi_a^r$ does not contribute to the correction. Both terms in the right-hand side of the matrix elements

$$\langle \Phi^{HF}|W|\Phi_a^r\rangle = \langle \Phi^{HF}|H_{el}|\Phi_a^r\rangle - \langle \Phi^{HF}|H_0|\Phi_a^r\rangle \tag{2.80}$$

are zero, the first one because of Brillouin's theorem and the second one because H_0 is diagonal in the basis of the Slater determinants. In addition, Slater determinants corresponding to triple excitations and higher level excitations do not contribute because the W operator only contains two-electron operators. Therefore, only doubly excited Slater determinants contribute to the second order energy correction.

The energies $E_j^{(0)}$ read

$$E_j^{(0)} = \langle \Phi_{ab}^{rs}|H_0|\Phi_{ab}^{rs}\rangle = E_0^{(0)} + \varepsilon_r + \varepsilon_s - \varepsilon_a - \varepsilon_b. \tag{2.81}$$

Therefore, using Eqs. (2.72) and (2.81), the second order correction to the energy reads

$$E^{\text{MP2}} = \sum_{a<b,r<s} \frac{|\langle \psi_a\psi_b|g_{12}|\psi_r\psi_s\rangle - \langle \psi_a\psi_b|g_{12}|\psi_s\psi_r\rangle|^2}{\varepsilon_a + \varepsilon_b - \varepsilon_r - \varepsilon_s}. \tag{2.82}$$

The MP2 method can be used to approximate the CISD energy of the ground state of a molecular system at a low computational cost. Higher order corrections have increasingly complicated expressions, however corrections up to fourth order (MP4) [27] are commonly available in the major quantum chemistry program packages.

As stated above, the CASSCF method is the method of choice to obtain a qualitative description of the electronic structure of a molecular system when static correlation plays a role. However, if a high accuracy is sought, the dynamic electronic correlation needs to be taken into account. Therefore, a method capable of describing accurately molecules in excited electronic states of different nature with a balanced accuracy over a wide range of geometries (in particular in regions where several electronic states become close in energy) must account for both the static and dynamics electronic correlations. The full CI and MRCISD method mentioned above can account for both types of correlation but they are extremely expansive and can only be applied to small systems. An alternative is to account for the dynamic electronic correlation energy through second-order perturbation theory on top of a CASSCF zeroth-order wavefunction. This is the idea behind the multi-reference perturbation theory methods (MRPT).

Several different methods of the MRPT2 type exist. The most popular are the multi-reference second-order Møller–Plesset (MRMP2) method of Hirao [28] and the complete active-space second-order perturbation theory (CASPT2) method of Andersson et al. [29]. In these methods, each state is perturbed separately. This can become problematic when, for instance, two states become sufficiently close in energy to interact after perturbation, these interactions will not be properly accounted for by such calculations. To solve this problem, methods based on second-order multi-state multi-reference perturbation theory (MS-MRPT2) can be used. These methods build an effective Hamiltonian between the perturbed states and diagonalize it, allowing one to treat quasi-degenerate states perturbatively. The most famous MS-MRPT2 methods are the multi-state CASPT2 method [30] and its extended version

(XMSCASPT2) [31], and the multi-configuration second-order quasi-degenerate perturbation theory (MCQDPT2) [32] and its extended version (XMCQDPT2) [33]. The XMCQDPT2 method is an approach to second order multi-state multi-reference perturbation theory recently developed by Granovsky, and implemented in the Firefly QC package [34], which is partially based on the GAMESS (US) source code [35]. It has been applied to a number of problems of biological and photochemical interest [36–43] and was shown to compare favourably with respect to experimental observations and other high-level theoretical methods [44–46]. All the excited state electronic structure calculations presented in this thesis have been performed with the CASSCF and XMCQDPT2 methods.

2.4 Potential Energy Surface Exploration

One of the most important applications of electronic structure calculations is the exploration of PESs. In particular, the theoretical description of chemical transformations requires the knowledge of the main stationary points of the relevant PESs.

For instance, a thermal reaction on the ground electronic state is, in the simplest case, characterized by the two minima corresponding to the reactants and products, and the transition state connecting them, as illustrated in the left panel of Fig. 2.4. Similarly, the characterization of stationary points is essential for the description of photochemical reactions. In this case, besides minima and transition states, conical intersections also play an important role. They provide channels connecting photoproducts on the ground state with the Franck–condon region on the excited state, as illustrated in the right panel of Fig. 2.4. As for the calculation of electronic wavefunctions and energies through (MC)SCF techniques, the determination of stationary points on PESs is an optimization problem.

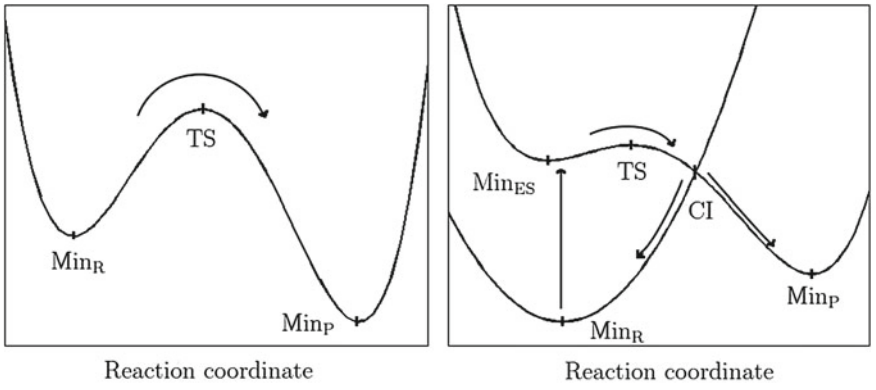

Fig. 2.4 Scheme illustrating a simple thermal reaction on the ground electronic state (*left panel*) and a photochemical reaction (*right panel*). Min_R and Min_P denote the minima corresponding to the reactants and products on the ground state PES. Min_{ES} denotes a local minimum on the excited state PES. TS denotes the transition state and CI denotes a point of conical intersection

2.4.1 Minima and Transition State Optimization

The simplest methods to find a minimum are methods based on the gradient of the energy with respect to the nuclear coordinates $\boldsymbol{g}(\boldsymbol{R_0}) = \nabla_{\boldsymbol{R}} E(\boldsymbol{R})|_{\boldsymbol{R}=\boldsymbol{R_0}}$. The steepest descent method uses the opposite of the gradient as the search direction $\boldsymbol{d}_i = -\boldsymbol{g}_i$, where the subscript i denotes the current iteration. A displacement is performed in this direction to find a new estimation of the minimum. At this point, a new gradient evaluation is performed, providing the search direction for the next step. This procedure is iterated until all the components of the gradient are smaller than a predefined threshold. A slightly more efficient method is the conjugated gradient method. In this method, the search direction is defined as a mixture of the opposite of the gradient and the previous search direction $\boldsymbol{d}_i = -\boldsymbol{g}_i + \beta_i \boldsymbol{d}_{i-1}$. Both methods are easy to implement but converge slowly towards a minimum.

A faster convergence can be obtained by using methods based on a second order expansion of the energy such as the Newton–Raphson-based methods [47]. In these methods, the search direction is defined as (see also Eq. (2.74))

$$\boldsymbol{d}_i = -\boldsymbol{H}_i^{-1} \boldsymbol{g}_i, \tag{2.83}$$

where $\boldsymbol{H}$ is the Hessian matrix of the electronic energy with respect to the nuclear coordinates. In a coordinate system that diagonalizes the Hessian matrix, the search direction reads

$$\boldsymbol{d'}_i = -(\boldsymbol{H}^{(\boldsymbol{d})})_i^{-1} \boldsymbol{g'}_i, \tag{2.84}$$

where $\boldsymbol{H}^{(\boldsymbol{d})}$ is the diagonal Hessian matrix. If all the eigenvalues of the Hessian matrix are positive, the algorithm converges towards a minimum, whereas if the Hessian has a negative eigenvalue, the algorithm tends to converge towards a transition state.

Two problems need to be addressed to make this class of methods robust and efficient. The first one is to improve the search direction and the size of the step taken along this direction. This can be done by adding a shift parameter λ in the Newton–Raphson step

$$\boldsymbol{d'}_i = -(\boldsymbol{H}^{(\boldsymbol{d})} - \lambda \boldsymbol{I})_i^{-1} \boldsymbol{g'}_i. \tag{2.85}$$

The shift parameter can be used to ensure that the optimization proceeds downhill even if the Hessian has negative eigenvalues. In addition, it can be chosen such that the step size is lower or equal to a predefined threshold. Popular methods using a shift parameter are the rational function optimization (RFO) [48] and Trust Radius (TR) methods [49, 50]. A finer control on the step size and direction can be achieved using an approximate line search method, which attempts to fit a polynomial function to the energies and gradients of the best previous points [51].

A second important issue is the calculation of the Hessian matrix which can be a computationally expansive task. A method to avoid such calculation is to start with an approximate Hessian, e.g. empirically determined or calculated at a lower level of theory, and to update the Hessian during the optimization using only energies and

gradients at successive optimization steps. The most popular updating scheme is the Broyden–Fletcher–Goldfarb–Shanno (BFGS) scheme [52–55]. Methods based on such an approximate Hessian matrix are called quasi-Newton methods.

The above methods can be modified to enforce convergence to a transition state. In this case, the quality of the initial geometry and Hessian are more crucial than for the optimization of a minimum.

The minimum and transition state optimizations performed in this thesis have been performed using the Berny algorithm [56] implemented in the Gaussian 03 program package [57].

2.4.2 Minimum Energy Conical Intersection Optimization

As mentioned in Sect. 2.2.3, a conical intersection is not an isolated point but a hyperline of $N-2$ dimensions (the seam of conical intersection), where N is the number of vibrational degrees of freedom. At each point of the seam, the degeneracy is lifted upon displacement in the branching plane whereas it is conserved at first order along the N-2 directions orthogonal to the branching plane. One is often interested in finding the point of lowest energy within this seam, called the minimum energy conical intersection (MECI) in order to characterize a photochemical process.

In this thesis, the method proposed by Bearpark et al. [58], and implemented in the Gaussian 03 package [57], has been used (see Chap. 3). Considering two adiabatic electronic states of energy E_1 and E_2, the principle of the method is to minimize simultaneously the energy difference $\Delta E = E_2 - E_1$ in the branching plane and the energy of the upper state E_2 in the intersection space. To avoid confusions in the notations, the gradient difference and derivative coupling vectors will be noted $\boldsymbol{x_1}$ and $\boldsymbol{x_2}$. The branching plane is the space spanned by the two unitary vectors $\boldsymbol{e}_{x_1}$ and $\boldsymbol{e}_{x_2}$ defined in Sect. 2.2.3. The condition for the minimization of the energy difference in the branching plane reads

$$\boldsymbol{\nabla}_R \Delta E^2 = 2\Delta E \boldsymbol{x_1}. \tag{2.86}$$

The squared energy difference is used because it varies more smoothly in the vicinity of a conical intersection. The norm of $\boldsymbol{x_1}$ has no significance, the step size should only depend on the energy difference ΔE, therefore the gradient to be used to minimize ΔE is defined as

$$\boldsymbol{f} = 2\Delta E \boldsymbol{e}_{x_1}. \tag{2.87}$$

The minimization of E_2 in the intersection space is done by mean of a projector

$$\boldsymbol{P} = \boldsymbol{I} - \boldsymbol{x_1}\boldsymbol{x_1}^T - \boldsymbol{x_2}\boldsymbol{x_2}^T. \tag{2.88}$$

In this case the gradient to be used is

$$\boldsymbol{g} = \boldsymbol{P}\boldsymbol{\nabla}_{\boldsymbol{R}} E_2. \tag{2.89}$$

Overall the MECI optimization uses the composite gradient

$$\bar{\boldsymbol{g}} = \boldsymbol{f} + \boldsymbol{g}. \tag{2.90}$$

Far from a conical intersection, the gradient is dominated by $\boldsymbol{f}$ and the algorithm converges towards a point of conical intersection. During this phase, the energies E_1 and E_2 can rise considerably and the algorithm can reach a portion of the conical intersection seam corresponding to highly distorted geometries. Therefore, as for transition state optimizations, the quality of the starting geometry is important. As the degeneracy is approached, $\boldsymbol{f}$ tends to zero and the gradient is dominated by $\boldsymbol{g}$. Therefore the algorithm minimizes the energy inside the conical intersection seam and converges towards the MECI.

2.4.3 Minimum Energy Paths Optimization

The knowledge of the main stationary points on the PESs of interest gives some information about the reactants, products and intermediates of a (photo)chemical reaction. However, a better insight into the mechanism behind this reaction can be obtained by computing the pathways linking these stationary points. Among the infinite number of paths connecting two points, the path requiring the least increase in energy is called the minimum energy path (MEP). The MEP usually follows the steepest descent path. However, this steepest descent path usually varies from a system of coordinates to another. When mass-weighted cartesian coordinates are used, the steepest descent path is also known as the intrinsic reaction coordinate (IRC). In this thesis, the algorithm of Gonzalez and Schlegel [59, 60], implemented in the Gaussian 03 program package [57], has been used.

From a starting geometry $\boldsymbol{R}_k$ with a gradient $\boldsymbol{g}_k$, the IRC algorithm optimizes a new point $\boldsymbol{R}_{k+1}$ such that the path between the two points is an arc of a circle to which both gradients $\boldsymbol{g}_k$ and $\boldsymbol{g}_{k+1}$ are tangent. Defining a step size s, the algorithm first generates a pivot point $\boldsymbol{R}^*_{k+1}$ at a distance $s/2$ of $\boldsymbol{R}_k$ along the direction of the gradient $\boldsymbol{g}_k$

$$\boldsymbol{R}^*_{k+1} = \boldsymbol{R}_k + \frac{s}{2}\frac{\boldsymbol{g}_k}{||\boldsymbol{g}_k||}. \tag{2.91}$$

The new point $\boldsymbol{R}_{k+1}$ is then obtained by a constrained optimization on the hypersphere of radius $s/2$ centered at $\boldsymbol{R}^*_{k+1}$.

References

1. H. Köppel, W. Domcke, L.S. Cederbaum, Mol. Phys. **43**, 851 (1981)
2. H. Köppel, W. Domcke, L.S. Cederbaum, Adv. Chem. Phys. **57**, 59 (1984)
3. G.A. Worth, L.S. Cederbaum, Annu. Rev. Phys. Chem. **55**, 127 (2004)
4. M. Born, R. Oppenheimer, Ann. Phys. **84**, 457 (1927)
5. M. Born, K. Huang, *The Dynamical Theory of Crystal Lattices* (Oxford University Press, Oxford, 1954)
6. W. Domcke, D.R. Yarkony, H. Köppel, *Conical Intersections, Electronic Strucutre, Dynamics and Spectroscopy* (World Scientific, New Jersey, 2004)
7. M.J. Paterson, M.J. Bearpark, M.A. Robb, L. Blancafort, J. Chem. Phys. **121**, 11562 (2004)
8. M.J. Paterson, M.J. Bearpark, M.A. Robb, L. Blancafort, G.A. Worth, Phys. Chem. Chem. Phys. **7**, 2100 (2005)
9. F. Sicilia, L. Blancafort, M.J. Bearpark, M.A. Robb, J. Phys. Chem. A **111**, 2182 (2007)
10. A. Szabo, N.S. Ostlund, *Modern Quantum Chemistry* (Mac Graw Hill Press, New York, 1989)
11. F. Jensen, *Introduction to Computational Chemistry* (Wiley, Chichester, 2007)
12. J.C. Slater, Phys. Rev. **34**, 1293 (1929)
13. D.R. Hartree, Proc. Camb. Philos. Soc. **24**, 88 (1928)
14. V. Fock, Z. Phys. **61**, 126 (1930)
15. E.U. Condon, Phys. Rev. **36**, 1121 (1930)
16. C.C.J. Roothaan, Rev. Mod. Phys. **23**, 69 (1951)
17. G.G. Hall, Proc. R. Soc. (Lond.) **A205**, 541 (1951)
18. R. Hoffmann, J. Chem. Phys. **39**, 1397 (1963)
19. J. Olsen, D.L. Yeager, P. Jorgensen, Adv. Chem. Phys. **54**, 1 (1983)
20. H.-J. Werner, Adv. Chem. Phys. **69**, 1 (1987)
21. R. Shepard, Adv. Chem. Phys. **69**, 63 (1987)
22. M.W. Schmidt, M.S. Gordon, Annu. Rev. Phys. Chem. **49**, 233 (1998)
23. J. Olsen, B.O. Roos, P. Jorgensen, H.J.A. Jensen, J. Chem. Phys. **89**, 2185 (1988)
24. M. Klene, M.A. Robb, L. Blancafort, M.J. Frisch, J. Chem. Phys. **119**, 713 (2003)
25. J. Ivanic, J. Chem. Phys. **119**, 9364 (2003), J. Chem. Phys. **119**, 9377 (2003)
26. C. Møller, M.S. Plesset, Phys. Rev. **46**, 618 (1934)
27. R. Krishnan, J.A. Pople, Int. J. Quant. Chem. **14**, 91 (1978)
28. K. Hirao, Chem. Phys. Lett. **190**, 374 (1992)
29. K. Andersson, P.A. Malmqvist, B.O. Roos, A.J. Sadlej, K. Wolinski, J. Phys. Chem. **94**, 5483 (1990)
30. J. Finley, P.-A. Malmqvist, B.O. Roos, L. Serrano-Andrés, Chem. Phys. Lett. **288**, 299 (1998)
31. T. Shiozaki, W. Györffy, P. Celani, H.-J. Werner, J. Phys. Chem. **135**, 081106 (2011)
32. H. Nakano, J. Chem. Phys. **99**, 7983 (1993)
33. A.A. Granovsky, J. Chem. Phys. **134**, 214113 (2011)
34. A.A. Granovsky, Firefly version 7.1.G, http://classic.chem.msu.su/gran/firefly/index.html
35. M.W. Schmidt, K.K. Baldridge, J.A. Boatz, S.T. Elbert, M.S. Gordon, J.H. Jensen, S. Koseki, N. Matsunaga, K.A. Nguyen, S. Su, T.L. Windus, M. Dupuis, J.A. Montgomery, J. Comput. Chem. **14**, 1347 (1993)
36. E. Epifanovsky, I. Polyakov, B. Grigorenko, A. Nemukhin, A.I. Krylov, J. Chem. Phys. **132**, 115104 (2010)
37. I.V. Polyakov, B.L. Grigorenko, E.M. Epifanovsky, A.I. Krylov, A.V. Nemukhin, J. Chem. Theory Comput. **6**, 2377 (2010)
38. B.L. Grigorenko, A.V. Nemukhin, D.I. Morozov, I.V. Polyakov, K.B. Bravaya, A.I. Krylov, J. Chem. Theory Comput. **8**, 1912 (2011)
39. B.L. Grigorenko, A.V. Nemukhin, I.V. Polyakov, A.I. Krylov, J. Phys. Chem. Lett. **4**, 1743 (2013)
40. P.M. Kozlowski, T. Kamachi, M. Kumar, T. Nakayama, K. Yoshizawa, J. Phys. Chem. B **114**, 5928 (2010)

41. A. Udvarhelyi, T. Domratcheva, J. Photochem. Photobiol. A **87**, 554 (2011)
42. I. Ioffe, A.L. Dobryakov, A.A. Granovsky, N.P. Ernsting, J.L. Pérez, Lustres. Chem. Phys. Chem. **12**, 1860 (2011)
43. A.V. Bochenkova, L.H. Andersen, Faraday Discuss. **163**, 297 (2013)
44. K. Kornobis, N. Kumar, B.M. Wong, P. Lodowski, M. Jaworska, T. Andruni, K. Ruud, P.M. Kozlowski, J. Phys. Chem. A **115**, 1280 (2011)
45. S. Gozem, M. Huntress, I. Schapiro, R. Lindh, A.A. Granovsky, C. Angeli, M. Olivucci, J. Chem. Theory Comput. **8**, 4069 (2012)
46. S. Gozem, F. Melaccio, R. Lindh, A.I. Krylov, A.A. Granovsky, C. Angeli, M. Olivucci, J. Chem. Theory Comput. **9**, 4495 (2013)
47. H.P. Hratchian, H.B. Schlegel, in *Theory and Applications of Computational Chemistry: The First 40 Years*, ed. by C.E. Dykstra, K.S. Kim, G. Frenking, G.E. Scuseria (Elsevier, Amsterdam, 2005), p. 195
48. A. Banerjee, A. Adams, J. Simons, R. Shepard, J. Chem. Phys. **89**, 52 (1985)
49. T. Helgaker, Chem. Phys. Lett. **182**, 503 (1991)
50. P. Culot, G. Dive, V.H. Nguyen, J.M. Ghuysen, Theor. Chim. Acta **82**, 189 (1992)
51. H.B. Schlegel, J. Comput. Chem. **3**, 214 (1982)
52. C.G. Broyden, IMA J. Appl. Math. **6**, 76 (1970)
53. R. Fletcher, Comput. J. **13**, 317 (1970)
54. D. Goldfarb, Math. Comput. **24**, 23 (1970)
55. D.F. Shanno, Math. Comput. **24**, 647 (1970)
56. C. Peng, P.Y. Ayala, H.B. Schlegel, M.J. Frisch, J. Comput. Chem. **17**, 49 (1996)
57. Gaussian 03, Revision C.02, M.J. Frisch, G.W. Trucks, H.B. Schlegel, G.E. Scuseria, M.A. Robb, J.R. Cheeseman, J.A. Montgomery, Jr., T. Vreven, K.N. Kudin, J.C. Burant, J.M. Millam, S.S. Iyengar, J. Tomasi, V. Barone, B. Mennucci, M. Cossi, G. Scalmani, N. Rega, G.A. Petersson, H. Nakatsuji, M. Hada, M. Ehara, K. Toyota, R. Fukuda, J. Hasegawa, M. Ishida, T. Nakajima, Y. Honda, O. Kitao, H. Nakai, M. Klene, X. Li, J.E. Knox, H.P. Hratchian, J.B. Cross, V. Bakken, C. Adamo, J. Jaramillo, R. Gomperts, R.E. Stratmann, O. Yazyev, A.J. Austin, R. Cammi, C. Pomelli, J.W. Ochterski, P.Y. Ayala, K. Morokuma, G.A. Voth, P. Salvador, J.J. Dannenberg, V.G. Zakrzewski, S. Dapprich, A.D. Daniels, M.C. Strain, O. Farkas, D.K. Malick, A.D. Rabuck, K. Raghavachari, J.B. Foresman, J.V. Ortiz, Q. Cui, A.G. Baboul, S. Clifford, J. Cioslowski, B.B. Stefanov, G. Liu, A. Liashenko, P. Piskorz, I. Komaromi, R.L. Martin, D.J. Fox, T. Keith, M.A. Al-Laham, C.Y. Peng, A. Nanayakkara, M. Challacombe, P.M.W. Gill, B. Johnson, W. Chen, M.W. Wong, C. Gonzalez, J.A. Pople, Gaussian Inc, Wallingford (2004)
58. M.J. Bearpark, M.A. Robb, H.B. Schlegel, Chem. Phys. Lett. **223**, 269 (1994)
59. C. Gonzalez, H.B. Schlegel, J. Chem. Phys. **90**, 2154 (1989)
60. C. Gonzalez, H.B. Schlegel, J. Phys. Chem. **94**, 5523 (1990)

http://www.springer.com/978-3-319-28978-6

Quantum Dynamics and Laser Control for Photochemistry

Sala, M.

2016, XIII, 189 p. 54 illus., 41 illus. in color., Hardcover
ISBN: 978-3-319-28978-6